Acta Cryst. (1978). B**34**, 3686–3690

The Electron and Proton Distribution in the Short O—H—O Bond in Hydrazinium Hydrogen Oxalate, $N_2H_5HC_2O_4$

BY JOHN O. THOMAS AND RUNE LIMINGA

Institute of Chemistry, University of Uppsala, Box 531, *S*-751 21 *Uppsala, Sweden*

(*Received* 22 *May* 1978; *accepted* 8 *August* 1978)

The room-temperature structure of hydrazinium hydrogen oxalate, $N_2H_5HC_2O_4$ ($C_2H_6N_2O_4$) [Thomas (1973). *Acta Cryst.* B**29**, 1767–1776], contains a short symmetric O—H—O bond (O···O: 2·457 Å) linking the $HC_2O_4^-$ ions. Fresh neutron data and earlier X-ray data are here used to derive the deformation electron and proton density in this bond. The static deformation electron density map exhibits a distinct electron-deficient region (peak height: −0·46 e Å^{-3}) at the centre of the bond, subtended on either side in the direction of the bond by regions of electron excess (peak height: +0·36 e Å^{-3}).

Introduction

The crystal structure of hydrazinium hydrogen oxalate was first solved by X-ray diffraction (Ahmed, Liminga & Olovsson, 1968); this was followed by a neutron diffraction study (Nilsson, Liminga & Olovsson, 1968) in which the hydrogen-bond scheme was investigated in greater detail. The centrosymmetric spatial distribution of the proton in the O—H—O bond between the oxalate groups was found to have a maximum at the bond centre (0,0,0). A more accurate X-ray study of $N_2D_5DC_2O_4$ and $N_2H_5HC_2O_4$ (Thomas, 1973) was aimed at observing the crystallographic isotope effect. Two intriguing features emerged. Firstly, the structure of $N_2D_5DC_2O_4$, though close to centrosymmetric, could be identified as having the space group $P2_1$ (in contrast to the space group $P2_1/m$ for $N_2H_5HC_2O_4$). That the mean structure of $N_2D_5DC_2O_4$ is truly non-centrosymmetric at room temperature has since been confirmed for a powder sample by a second harmonic generation test (Dougherty & Kurtz, 1976). A signal ~1% of that from quartz was obtained, whereas $N_2H_5HC_2O_4$ produced a null signal, indicative of a valid crystallographic symmetry centre.

It was also observed (Thomas, 1973) that the average electron distribution associated with the H atom of the short symmetric O—H—O bond (O···O: 2·457 Å) had a dumb-bell-shaped double maximum lying across the origin, with peaks in such positions as to suggest a 50%–50% statistical superposition of an O—H···O and an O···H—O bond [Figs. 1 and 2(*a*)]. This was in contrast to the single almost spherical peak found for the proton in the earlier neutron study.

At about the same time similar diffraction results were obtained for short O—H—O bonds in potassium hydrogen *meso*-tartrate (Kroon & Kanters, 1972), potassium hydrogen succinate (McAdam, Currie & Speakman, 1971) and potassium hydrogen bis-(trifluoroacetate) (Macdonald, Speakman & Hadži, 1972). It was proposed that this apparent anomaly be referred to as the KKM (Kanters–Kroon–McAdam) effect.

In view of the improved quality of the neutron diffraction data now available at Studsvik compared with that at the time of the first $N_2H_5HC_2O_4$ study, it was felt worthwhile to reexamine the form of the proton distribution and to investigate the appearance of an *X*–*N* deformation electron density map for a short symmetric O—H—O bond. Such bonds are interesting

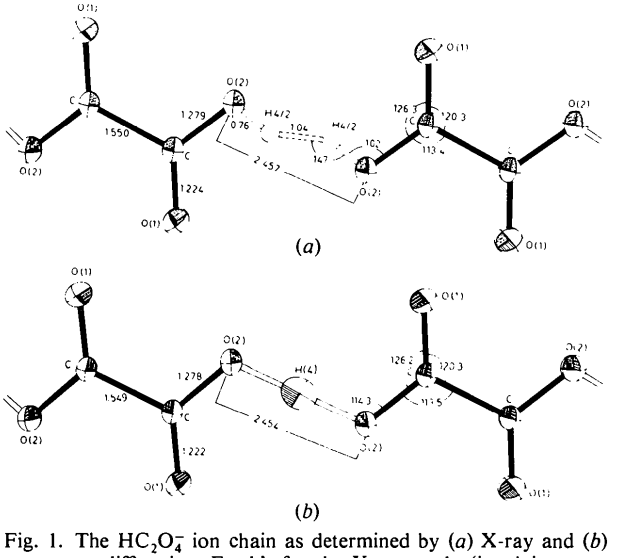

Fig. 1. The $HC_2O_4^-$ ion chain as determined by (*a*) X-ray and (*b*) neutron diffraction. E.s.d.'s for the X-ray study (involving non-hydrogen atoms only) are 0·001–0·002 Å for the distances and 0·10° for the angles. E.s.d.'s for the neutron study are 0·001 Å for the distances and 0·06–0·09° for the angles. Thermal ellipsoids are drawn to include 50% probability.

as they have been suggested as the structural feature responsible for various types of critical phenomena in the solid state, typically ferroelectric phase transitions.

Crystal data

Hydrazinium hydrogen oxalate, $N_2H_5HC_2O_4$ ($C_2H_6N_2O_4$), FW 122·09, monoclinic, $P2_1/m$, a = 3·5792 (3), b = 13·3228 (16), c = 5·0965 (3) Å, β = 102·600 (6)°, V = 237·177 Å^3 at 298 K, Z = 2, D_x = 1·709 g cm^{-3}, μ_c(Mo $K\alpha$) = 1·774 cm^{-1}, μ_o (for 1·210 Å neutrons) = 2·18 cm^{-1}.

Experimental

All features relevant to the X-ray data used here are discussed in Thomas (1973). The following points can be repeated: the data were collected on a Stoe–Philips four-circle diffractometer with graphite-monochromatized Mo $K\alpha$ radiation out to sin θ/λ = 0·7035 Å^{-1}. The final data set comprised 707 independent reflexions, of which 632 had $F^2 > 2\sigma(F^2)$; these were used in the refinement. The only treatment found to be needed for secondary extinction was the exclusion of $(10\bar{1})$ (the strongest in the data set).

The neutron data were collected at 295 K on a PDP-8-controlled Hilger & Watts four-circle diffractometer at the R2 reactor at Studsvik, Sweden. The neutron beam had a mean wavelength of 1·210 Å after passing through a double-crystal monochromator (Stedman, Almqvist, Raunio & Nilsson, 1969), and a flux at the crystal of 1·26 × 10^6 n cm^{-2} s^{-1}. The crystal used for the data collection (volume: 95 mm^3) was grown in the same way as the X-ray crystal, and had three pairs of parallel faces $(0,0,\pm1)$; $\mp1,0,\pm1$; and $0,\pm1,0)$; separations 7·4, 4·2 and 2·8 mm, respectively. A complete quadrant of data was collected out to sin θ/λ = 0·66 Å^{-1} with an $\omega/2\theta$ scan mode and a background–peak–background measurement procedure. 742 independent reflexions resulted, of which all but 28 most strongly affected by extinction were used in the refinement.

The data were corrected for Lorentz, absorption and secondary-extinction effects. μ was measured experimentally as 2·18 cm^{-1}. Transmission factors were in the range 0·38–0·58.

Refinement

The refinement of the neutron data was begun with the positional and thermal parameters from the X-ray study (Tables 1 and 2) as starting values. This model, with H(4)/2 displaced from the origin, produced unstable refinements which could only be stabilized by

Table 1. *Neutron diffraction determined positional parameters* (×10^5) *from the present study* (*upper row*), *compared with earlier X-ray values* (*Thomas*, 1973)

	x	y	z
C	61892 (17)	2501 (4)	62849 (12)
	61894 (28)	2499 (7)	62876 (17)
N(1)	29382 (23)	25000	8146 (16)
	29543 (45)	25000	8132 (30)
N(2)	10307 (20)	25000	30086 (16)
	10308 (44)	25000	30121 (30)
O(1)	58979 (27)	11500 (6)	66607 (16)
	58959 (26)	11514 (6)	66648 (16)
O(2)	83708 (25)	−3620 (5)	78386 (17)
	83703 (25)	−3644 (6)	78385 (15)
H(1)	20500 (82)	18808 (18)	−3032 (51)
	22200 (600)	19800 (200)	−400 (400)
H(2)	19678 (61)	18741 (15)	41677 (43)
	18800 (500)	19500 (200)	39400 (400)
H(3)	−19502 (72)	25000	23442 (77)
	−12600 (900)	25000	25100 (500)
H(4)*	0	0	0
	7000 (1300)	300 (500)	10000 (800)

* H(4) disordered in X-ray refinement.

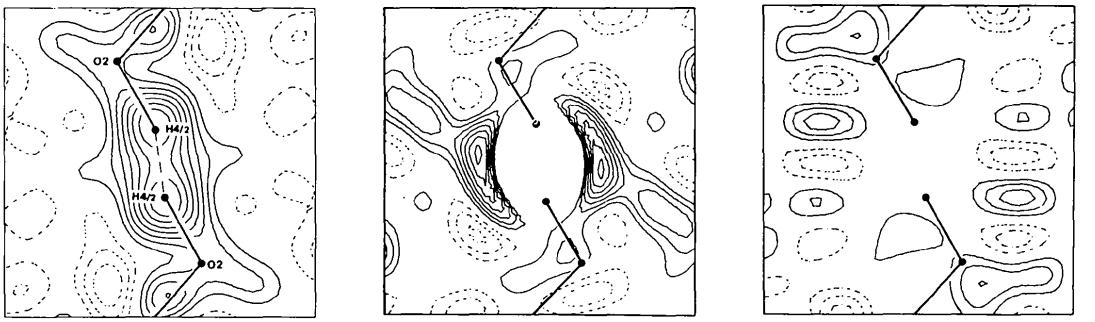

(*a*) (*b*) (*c*)

Fig. 2. Difference syntheses for the O–H–O bond in $N_2H_5HC_2O_4$. (*a*) X-ray $F_o - F_c$ synthesis with H(4) omitted from F_c. Contour interval: 0·05 e Å^{-3}. (*b*) Neutron $F_o - F_c$ synthesis with H(4) omitted from F_c. Contour interval: 0·05 p Å^{-3}. Central trough not plotted. (*c*) Neutron $F_o - F_c$ synthesis with H(4) included in F_c. Contour interval: 0·025 p Å^{-3} and zero contour omitted for all maps.

fixing H(4) at the origin. This confirmed the findings of the earlier neutron study. In the final refinement, made with the full-matrix least-squares program *UPALS*, the function minimized was $\sum w(|F_o|^2 - |F_c|^2)^2$, where $w = 1/\sigma(F^2)$, and (*a*) $\sigma^2(F^2) = \sigma^2_{\text{count}}(F^2) + (0{\cdot}05F^2)^2$ for $F^2 > L$, and (*b*) $\sigma^2(F^2) = \sigma^2_{\text{count}}(F^2) + [0{\cdot}05(2L - F^2)]^2$ for $F^2 < L$, where L is the value of F^2 (here 1·2) below which the reflexion can be considered weak. A type 1 anisotropic model for secondary extinction (Coppens & Hamilton, 1970) was chosen as giving the better representation. In the final refinement, 28 reflexions were deleted for which $F^2_{\text{corr}}/F^2_o > 2{\cdot}25$, where F_{corr} is the structure factor after correction for extinction.

The final extinction parameters were: $Z'_{11} = 1{\cdot}13\ (10)$, $Z'_{22} = 1{\cdot}56\ (17)$, $Z'_{33} = 0{\cdot}30\ (4)$, $Z'_{12} = 0{\cdot}42\ (18)$, $Z'_{13} = -0{\cdot}07\ (8)$ and $Z'_{23} = 0{\cdot}14\ (10)$.

Agreement factors obtained were:

$$R(F^2) = \sum |F_o^2 - F_c^2| / \sum |F_o^2| = 0{\cdot}047,$$

$$R_w(F^2) = (\sum w|F_o^2 - F_c^2|^2 / \sum wF_o^4|)^{1/2} = 0{\cdot}054,$$

$$R(F) = 0{\cdot}037.$$

The coherent neutron scattering amplitudes were: $b_O = 5{\cdot}80$, $b_N = 9{\cdot}40$, $b_C = 6{\cdot}65$ and $b_H = 3{\cdot}74$ fermi (Bacon, 1972). All calculations were made on IBM 370/155 or IBM 1800 machines with programs described by Lundgren (1976).

Final positional and thermal parameters from the earlier X-ray and the present neutron study are compared in Tables 1 and 2.* The resulting geometries associated with the $HC_2O_4^-$ ion chains are compared in Fig. 1.

The following series of maps have been calculated for the O–H–O bond:

(*a*) An X-ray $F_o - F_c$ difference map with H(4) omitted in the refinement. The section plotted in Fig. 2(*a*) is the plane passing through the origin, O(2) and H(4)/2 (X-ray coordinates).

(*b*) The corresponding neutron $F_o - F_c$ difference map, plotted in Fig. 2(*b*) for the same plane.

(*c*) A neutron $F_o - F_c$ difference map (Fig. 2*c*) after the final neutron refinement (Table 1).

* A list of structure factors has been deposited with the British Library Lending Division as Supplementary Publication No. SUP 33864 (6 pp.). Copies may be obtained through The Executive Secretary, International Union of Crystallography, 5 Abbey Square, Chester CH1 2HU, England.

Table 3. *The multipole deformation density model refined for* $N_2H_5HC_2O_4$ *after Hirshfeld* (1971)

The static deformation density is expressed as $\sum_{n,k} c_{nk}\varphi_{nk}(r,\theta)$, where the c_{nk}'s are refinable deformation coefficients. The deformation functions used, φ_{nk}, have the general form $N_n r^n e^{-\gamma r} \cos^n\theta_k$, where N_n is a normalization factor, n is an integer between 0 and 4, θ_k is the angle between **r** and the kth of a chosen set of polar axes, and γ is a parameter governing the breadth of the deformation function. The dynamic deformation density is obtained from the static density by applying the refined thermal parameters.

	Point symmetry	Number of deformation density functions
N(1)	*m*	22
N(2)	*m*	22
C	*m*	22
O(1)	*m*	22
O(2)	*m*	22
H(1)	rotation	6
H(2)	rotation	6
H(3)	rotation	6
H(4)	rotation + symmetry centre	3
	Total:	131

Table 2. *Neutron diffraction determined anisotropic thermal parameters* ($\times 10^4$) *from the present study (upper row), compared with the earlier X-ray values (Thomas, 1973)*

The form of the temperature factor is: $\exp[-(\beta_{11}h^2 + \cdots + 2\beta_{12}hk + \cdots)]$. The r.m.s. components ($R_i \times 10^3$ Å) of thermal displacement along the principal axes of the thermal vibration ellipsoids are also given.

	β_{11}	β_{22}	β_{33}	β_{12}	β_{13}	β_{23}	R_1	R_2	R_3
C	430 (5)	18 (1)	110 (3)	6 (1)	−34 (3)	−13 (4)	108 (2)	128 (1)	180 (1)
	408 (8)	22 (1)	108 (3)	2 (1)	−17 (4)	−3 (1)	110 (2)	141 (2)	171 (2)
N(1)	621 (7)	27 (1)	233 (3)	0	110 (4)	0	155 (1)	167 (1)	196 (1)
	635 (13)	26 (1)	215 (5)	0	114 (6)	0	152 (2)	160 (2)	199 (2)
N(2)	485 (7)	23 (1)	286 (3)	0	128 (4)	0	145 (1)	163 (1)	193 (1)
	438 (12)	23 (1)	266 (6)	0	112 (6)	0	145 (2)	157 (2)	185 (2)
O(1)	783 (8)	20 (1)	193 (3)	21 (1)	−99 (4)	−16 (1)	121 (1)	144 (1)	251 (1)
	793 (9)	22 (1)	200 (3)	20 (1)	−92 (4)	−16 (1)	128 (2)	149 (1)	251 (1)
O(2)	623 (7)	21 (1)	160 (3)	13 (1)	−116 (4)	−3 (1)	115 (2)	137 (1)	231 (1)
	643 (8)	23 (1)	160 (3)	13 (1)	−123 (4)	−5 (1)	114 (2)	144 (1)	235 (1)
H(1)	1535 (26)*	53 (1)	418 (9)	−57 (4)	227 (13)	−62 (3)	171 (3)	256 (3)	314 (3)
H(2)	1042 (17)	43 (1)	425 (8)	27 (3)	264 (10)	39 (2)	175 (2)	220 (2)	269 (2)
H(3)	568 (19)	57 (1)	610 (16)	0	209 (14)	0	179 (3)	226 (3)	277 (3)
H(4)	762 (16)	33 (1)	313 (9)	14 (4)	23 (10)	14 (2)	164 (3)	197 (3)	232 (3)

* The r.m.s. amplitudes for H(1), ..., H(4) from the X-ray study were: 0·23 (1), 0·20 (1), 0·19 (2) and 0·25 (3) Å, respectively.

(*d*) An *X–N* difference map (Fig. 3*a*) calculated with the neutron diffraction positional and thermal parameters from the present study and earlier X-ray data [with $10\bar{1}$ and $F^2 < 2\sigma(F^2)$ removed] (Coppens, 1974).

(*e*) Dynamic and static multipole deformation density maps (Fig. 3*b*,*c*) calculated with the model of Hirshfeld (1971) to describe the electron deformation, with positional and thermal parameters fixed to their neutron diffraction values. The deformation model refined is summarized in Table 3.

X–N and multipole deformation densities for the entire $HC_2O_4^-$ ion have also been calculated and are given in Fig. 4.

Discussion

The present discussion is concerned primarily with the electron and proton distribution in the short O–H–O bond linking the $HC_2O_4^-$ ions.

The O–H–O *bond*

The apparent contradiction in the models derived from the X-ray and neutron data (Fig. 1) can be reconciled in that the centroid of the electron distribution associated with the H atom in an *X*–H bond is 0·1–0·2 Å nearer atom *X* than the centroid of the corresponding proton distribution. In a disordered hydrogen bond, assumed to be a 50%–50% statistical overlap of O–H···O and O···H–O, the centroids of the electron distributions associated with the two disordered H-atom positions can thus be as much as 0·4 Å further apart – and hence resolvable in an X-ray experiment (Fig. 2*a*) – than the corresponding centroids in the disordered proton distributions. In the present case, the disordered proton positions will be only ~0·25 Å apart (across the origin) and will be observed as an unresolved central peak [omitted from Fig. 2(*b*)] in the present neutron experiment. A similar central peak was also found in the earlier poorer quality neutron study (see Fig. 2 of Nilsson, Liminga & Olovsson, 1968). It is thus misleading to invoke such a term as KKM effect to characterize the above situation, although it is unclear how the positive peaks on either side of the O···O bond in Fig. 2(*b*) can be related to the proton distribution in the bond. Similar spurious positive and negative peaks appear in the neutron $F_o - F_c$ residue map (Fig. 2*c*).

The most striking feature of the *X–N* map for the O–H–O bond (Fig. 3*a*) is the large region of charge depletion at the centre of the bond. This may be compared with the recent result for the slightly shorter

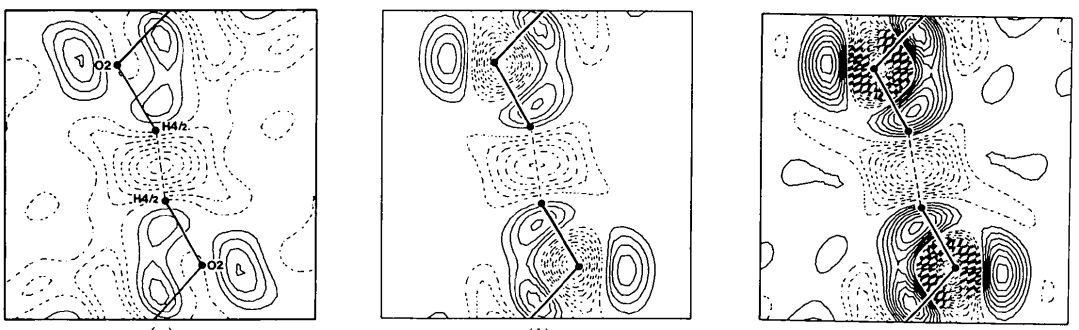

(*a*) (*b*) (*c*)

Fig. 3. Difference and deformation density maps for the O–H–O bond in $N_2H_5HC_2O_4$. (*a*) *X–N*, (*b*) dynamic multipole deformation density, (*c*) static multipole deformation density. Contour interval: 0·05 e Å^{-3} and zero contour omitted for all maps.

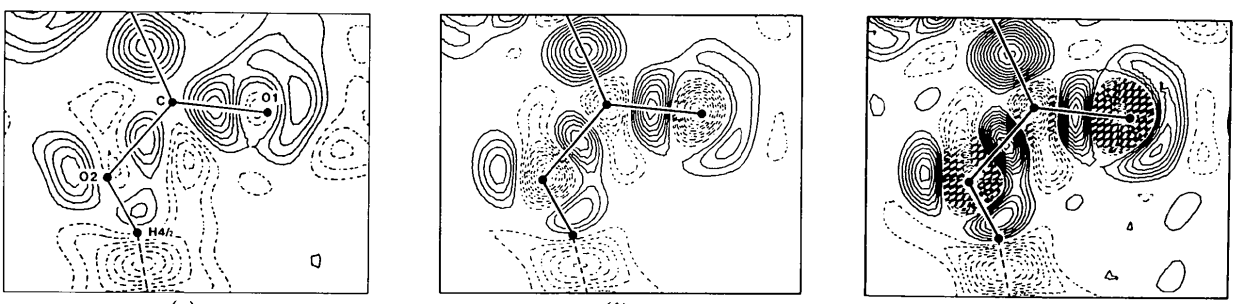

(*a*) (*b*) (*c*)

Fig. 4. Difference and deformation electron density maps for the $HC_2O_4^-$ ion in $N_2H_5HC_2O_4$. (*a*) *X–N* map, (*b*) dynamic and (*c*) static multipole deformation density map. Contour interval: 0·05 e Å^{-3} and zero contour omitted for all maps.

2·44 Å O–H–O bond in sodium hydrogen diacetate (Stevens, Lehmann & Coppens, 1977) where no significant charge depletion was found at the centre of the bond. It is known, however, that hydrogen bonds undergo a gradual change in character across the O···O distance range 2·40–2·50 Å, from truly centred at the lower limit (with two equivalent O–H distances of 1·2 Å) to asymmetric (O–H···O type) at the upper value. The asymmetric bond type is characterized by a difference density minimum in the H···O bond (Tellgren, Thomas & Olovsson, 1977). It is reasonable then (regarding the O–H–O bond in $N_2H_5HC_2O_4$ as a 50%–50% statistical overlap of O–H···O and O···H–O) that the difference density map should show a charge diminution at the bond centre. The covalent density remaining in the O–H bonds [peak heights 0·36 e Å^{-3} in the static deformation density of Fig. 3(*c*)] must be seen as an overlap of O–H covalent bond density and lone-pair density associated with the O atom acceptor site. Both contributions can be expected to be somewhat diminished through the formation of the hydrogen bond on the basis of the recent study of the hydrogen-bonded system $(CH_3)_2NH_2HC_2O_4$ (Thomas, 1977). The central trough in the bond falls to −0·46 e Å^{-3} in the static deformation density of Fig. 3(*c*).

In both Figs. 3 and 4, deep troughs occur at the non-hydrogen nuclear positions in the deformation density maps. These are presumably related to imprecision in the neutron-determined thermal parameters. Such errors inhibit any attempt to make an accurate assessment of electron density in the vicinity of the nuclei (Stewart, 1968). That no corresponding troughs appear in the *X–N* maps can be a result of the use of different scale factors in the two cases. This does not imply that the *X–N* maps are in any way more reliable at the nuclei, however.

The $HC_2O_4^-$ *ion*

We see that the *X–N* map for the $HC_2O_4^-$ ion (Fig. 4*a*) is well reproduced by the thermally smeared refined multipole deformation model (Fig. 4*b*). Some of the features appearing in the maps should, nevertheless, be taken as a warning of the possible dangers inherent in making too sophisticated an interpretation of *X–N* difference maps obtained from room-temperature data. The present behaviour may, however, be an artefact of the statistical disorder in the system. Two features can be remarked upon in particular in this connexion:

(*a*) An apparently higher covalent bond density in C–O(1) compared with C–O(2) in Fig. 4(*a*) gives way to a reversal in the effect (at least in the peak heights: 0·40 and 0·50 e Å^{-3}, respectively) in the static deformation density of Fig. 4(*c*).

(*b*) Similarly, the position of the lone-pair density peak on O(1) as seen in Fig. 4(*a*) is shifted significantly in the dynamic and static deformation density maps (Figs. 4*b*,*c*).

The authors thank Professor I. Olovsson, leader of the Hydrogen-Bond Project at this Institute, and Dr R. Tellgren for his help with the neutron diffraction part of the study. This work has been financed by grants from the Swedish Natural Science Research Council.

References

AHMED, N. A., LIMINGA, R. & OLOVSSON, I. (1968). *Acta Chem. Scand.* **22**, 88–96.
BACON, G. E. (1972). *Acta Cryst.* A**28**, 357–358.
COPPENS, P. (1974). *Acta Cryst.* B**30**, 255–261.
COPPENS, P. & HAMILTON, W. C. (1970). *Acta Cryst.* A**26**, 71–83.
DOUGHERTY, J. P. & KURTZ, S. K. (1976). *J. Appl. Cryst.* **9**, 145–158.
HIRSHFELD, F. L. (1971). *Acta Cryst.* B**27**, 769–781.
KROON, J. & KANTERS, J. A. (1972). *Acta Cryst.* B**28**, 714–722.
LUNDGREN, J.-O. (1976). *Crystallographic Computer Programs*. Report UUIC-B13-4-03. Institute of Chemistry, Univ. of Uppsala, Sweden.
MCADAM, A., CURRIE, M. & SPEAKMAN, J. C. (1971). *J. Chem. Soc. A*, pp. 1994–1997.
MACDONALD, A. L., SPEAKMAN, J. C. & HADŽI, D. (1972). *J. Chem. Soc. Perkin Trans.* 2, pp. 825–835.
NILSSON, Å., LIMINGA, R. & OLOVSSON, I. (1968). *Acta Chem. Scand.* **22**, 719–731.
STEDMAN, R., ALMQVIST, L., RAUNIO, G. & NILSSON, G. (1969). *Rev. Sci. Instrum.* **40**, 249–255.
STEVENS, E. D., LEHMANN, M. S. & COPPENS, P. (1977). *J. Am. Chem. Soc.* **99**, 2829–2831.
STEWART, R. F. (1968). *Acta Cryst.* A**24**, 497–505.
TELLGREN, R., THOMAS, J. O. & OLOVSSON, I. (1977). *Acta Cryst.* B**33**, 3500–3504.
THOMAS, J. O. (1973). *Acta Cryst.* B**29**, 1767–1776.
THOMAS, J. O. (1977). *Acta Cryst.* B**33**, 2867–2876.